First-principles calculation of hot-electron scattering in metals

Florian Ladstädter, Ulrich Hohenester,* Peter Puschnig,† and Claudia Ambrosch-Draxl
Institut für Physik, Karl-Franzens-Universität Graz, Universitätsplatz 5, 8010 Graz, Austria
(Received 25 June 2004; revised manuscript received 24 September 2004; published 23 December 2004)

We analyze hot-electron scatterings in metals within a first-principles approach based on density-functional-theory band-structure calculations and on Green-function calculations within the *GW* approximation. Results for hot-electron lifetimes and the differential cross section of the underlying scattering process are presented for Al, Cu, Au, and Pd, and analyzed with emphasis on the differences and similarities with respect to the predictions of the homogeneous electron-gas model. The electron-gas results can nicely explain the scattering characteristics in aluminium, whereas in copper and gold a strong enhancement of the hot-electron lifetimes is found and attributed to *d*-band screening. Finally, in palladium *d*-band scatterings are responsible for a drastic modification of the scattering characteristics, which no longer can be explained by the homogeneous electron-gas results.

DOI: 10.1103/PhysRevB.70.235125 PACS number(s): 71.10.Ca, 72.15.Lh, 72.10.−d, 71.15.Mb

I. INTRODUCTION

Over many decades the understanding of metals as prototypical many-particle systems has led to numerous theoretical efforts. Only many-body perturbation theory, which was originally developed in the field of quantum electrodynamics, finally allowed one to describe the basic characteristics of electron dynamics in metals within the normal state:[1–5] while electrons with excess energies slightly above the Fermi level can be approximately treated as independent particles with almost infinite lifetimes, states at higher energies become short lived because of Coulomb renormalizations which can be effectively described by electron-electron scatterings. Although the basic features of such hot-electron lifetimes can be already grasped from the solutions of the homogeneous electron-gas model,[1–5] for real metals the more complex band structure is expected to have a decisive influence. The advent of *ab-initio* techniques, e.g., density-functional theory, brought a new facet to modern solid-state research, as they allowed to calculate such decisive material properties within a true first-principles manner. Echenique and co-workers[6–12] were the first to derive within a combined first-principles band-structure and many-body perturbation theory framework the hot-electron lifetimes for real metals, and to demonstrate the importance of band-structure effects. Their work, based on the Green function formalism within the *GW* approximation,[13–15] revealed a substantial enhancement of hot-electron lifetimes in noble metals attributed to *d*-band screening, and lifetime anisotropies attributed to the genuine solid-state band structure. These findings were supported by other work,[16–20] which addressed in more detail effects associated to, e.g., energy or quasiparticle renormalizations.

An accurate knowledge of hot-electron lifetimes in metals is of paramount importance for the understanding of a variety of important physical and chemical phenomena, ranging from surface chemistry to the design of devices based on metal-semiconductor junctions. However, the experimental knowledge of hot-electron lifetimes τ due to electron-electron scatterings is still far from being complete. This somewhat surprising situation stems from the difficulties to extract τ from experiment. All available techniques, such as, e.g., transport,[21] photoemission, inverse photoemission,[22] two-photon photoemission,[23] and ballistic electron emission spectroscopy[24,25] only provide indirect information of τ, which then has to be extracted by support of a sufficiently sophisticated theory. Each technique has its own advantages and disadvantages. For instance, Flores and co-workers[20,25–28] theoretically analyzed the role of hot-electron scatterings in ballistic electron emission spectroscopy and demonstrated the sensitivity of this technique for the extraction of accurate τ values in metals. In Ref. 20 hot-electron lifetimes of gold and palladium were obtained from experimental data,[29,30] and shown to be in excellent agreement with the results of first-principles calculations. An assumption implicitly made in this work is that the hot electron loses in electron-electron scatterings a substantial fraction of its excess energy. Also in the analysis of other experimental techniques, such as two-photon photoemission,[23] the final state of the hot electron as well as that of the scattering partner has a decisive impact on the deconvolution procedure to extract τ. Quite generally, such details of the scattering process require a careful analysis of both, the hot-electron lifetimes and of the differential cross section of the scattering.

It is the purpose of this paper to analyze within a first-principles approach based on density-functional-theory band-structure calculations and on many-body perturbation theory the lifetimes of hot electrons in metals and the differential cross sections of the underlying electron-electron scatterings. To our best knowledge, no corresponding analysis has hitherto been reported in the literature. In our theoretical approach we extend the framework presented in Ref. 20, where we obtained hot-electron lifetimes from a *GW* approximation calculation of the quasiparticle lifetimes based on band-structure results obtained within the local-density approximation and with a linearized-augmented-plane-wave (LAPW) basis.[31] Our paper has been organized as follows. In Sec. II we briefly describe our theoretical approach, and provide evidence that the *GW* self-energy can be interpreted in terms of a scattering process. Section III provides details of our computational scheme, and we present results for the

hot-electron scatterings in aluminium, copper, gold, and palladium. More specifically, we investigate differences and similarities of our first-principles calculations with respect to the predictions of the homogeneous electron-gas model, and elucidate the role of *d*-band screening in copper and gold and of *d*-band scatterings in palladium. Finally, in Sec. IV we draw some conclusions.

II. THEORY

Band structure calculations based on density-functional theory provide us with the eigenenergies E_n and functions $\phi_n(\boldsymbol{r})$ characterizing the solid-state ground state.[32] Although not strictly justified, they are conveniently also interpreted as excited-state properties. For instance, one additional hot electron injected above the Fermi energy into a metal has the approximate energy E_i and wave function $\phi_i(\boldsymbol{r})$. The most obvious shortcoming of this interpretation is the lack of scatterings: because E_i is entirely real, an electron placed in this state will stay there forever. On general physical grounds we expect that the hot electron will suffer scatterings with the electrons of the metal and hereby lose energy. Many-body perturbation theory is a convenient tool for the description of such scatterings.[4,5] Within the framework of the celebrated *GW* approach,[13–15] to the lowest order of approximation the hot-electron lifetimes can be computed from the imaginary part of the *GW* self-energy according to[6–8,16,33]

$$\tau_i^{-1} = \frac{1}{\pi^2}\sum_f \int_{\mathrm{BZ}} d\boldsymbol{q} \sum_{\boldsymbol{G}.\boldsymbol{G}'} \frac{B_{if}(\boldsymbol{q}+\boldsymbol{G})B_{if}^*(\boldsymbol{q}+\boldsymbol{G}')}{|\boldsymbol{q}+\boldsymbol{G}|^2} \times \mathrm{Im}[-\epsilon_{\boldsymbol{G}.\boldsymbol{G}'}^{-1}(\boldsymbol{q}, E_i - E_f)]. \quad (1)$$

Here, $\boldsymbol{q}$ is a wave vector within the first Brillouin zone, $\boldsymbol{G}$ and $\boldsymbol{G}'$ are reciprocal lattice wave vectors, E_i is the energy of the initial state of the hot electron, the sum extends over all states f whose energies E_f are above the Fermi energy and below E_i, B_{if} is the hot-electron overlap matrix element for a given wave vector [for details see Eq. (6)], and, finally, ϵ is the dielectric function calculated within the usual random-phase approximation. Equation (1) accounts for the fact that a single-electron excitation is not a stationary state of the combined system hot electron plus electrons of the metal, and thus becomes attenuated through inelastic scatterings. It might betempting to interpret f as the final states of the scattering. This, however, is not directly backed by the *GW* approach itself which only allows for the calculation of the complex self-energy, whose imaginary part is closely related to τ^{-1}, but provides no clear answer regarding the meaning of the states f. Yet, the scattering-type interpretation of Eq. (1) in terms of initial and final scattering states is sound. To see that, we adopt a simple density-matrix description[34] instead of the more complicated framework of nonequilibrium Green functions. Let $H_0 = \Sigma_k E_k c_k^\dagger c_k$ be the Hamiltonian of single-particle excitations, where c_k is the fermionic field operator associated to the single-particle excitation k, and H_1 the Hamiltonian of those Coulomb couplings which are not included in the band-structure calculation and which will be treated by means of perturbation theory. Suppose that initially the system is in the state $|i\rangle = c_i^\dagger|0\rangle$ with $|0\rangle$ the metal ground state. What we shall do next is to introduce the projection operators $\mathbb{P} = |i\rangle\langle i|$ and $\mathbb{Q} = \mathbb{1} - \mathbb{P}$ which project on state i and on the remainder, respectively, and to separate the Coulomb couplings into $H_1 = (\mathbb{P}H_1\mathbb{Q} + \mathbb{Q}H_1\mathbb{P}) + \mathbb{Q}H_1\mathbb{Q} = H' + H''$, where H' accounts for the Coulomb couplings between the hot electron i and the other electrons, and H'' for the remainder. We have dropped the self-interaction term $\mathbb{P}H_1\mathbb{P}$ which is already included in H_0. With this at hand, we can now approximately describe the scattering process by introducing an interaction representation according to $H_0 + H''$ and treating the scattering within lowest order perturbation theory of H', i.e., in the so-called Born approximation. We denote the density operator of the system with ρ, whose time evolution is given by the Liouville von-Neumann equation[35,36] $\dot{\rho}(t) = -i[H'(t), \rho(t)]$ subject to the initial condition $\rho_0 = |i\rangle\langle i|$. Within this scheme,

$$\dot{\rho}(t) \cong -\int_{t_0}^{t} dt' [H'(t), [H'(t'), \rho_0]] \quad (2)$$

describes the approximate time evolution of the density operator.[37] The term on the right-hand side has the intriguing structure that at time t' the hot electron and the metal electrons become correlated through $H'(t')$, the correlated system propagates for a while [note that $H'(t)$ is given in the interaction representation according to H_0 and H''], and finally a back-action on the hot electron occurs at time t. Because of the finite interaction time the hot electron can exchange energy with the metal electrons. In evaluating the double commutator in Eq. (2) we describe the Coulomb coupling in the random-phase approximation[38–40]

$$H' \cong \int d\boldsymbol{r} d\boldsymbol{r}' \frac{\hat{n}'(\boldsymbol{r})\hat{n}''(\boldsymbol{r}')}{|\boldsymbol{r} - \boldsymbol{r}'|}, \quad (3)$$

where $n'(\boldsymbol{r})$ describes those density fluctuations that affect particle i and $\hat{n}''(\boldsymbol{r}')$ the remaining ones, and assume that the density fluctuations $n'(\boldsymbol{r})$ and $\hat{n}''(\boldsymbol{r}')$ move independently of each other. As discussed in more detail in the Appendix, for the distribution function $n_i = \langle c_i^\dagger c_i \rangle$ we then obtain the Boltzmann-like equation of motion

$$\dot{n}_i \cong \frac{1}{\pi^2}\sum_f \int_{\mathrm{BZ}} d\boldsymbol{q} \sum_{\boldsymbol{G}.\boldsymbol{G}'} \Bigg(-\frac{B_{if}(\boldsymbol{q}+\boldsymbol{G})B_{if}^*(\boldsymbol{q}+\boldsymbol{G}')}{|\boldsymbol{q}+\boldsymbol{G}|^2} \times \mathrm{Im}[-\epsilon_{\boldsymbol{G}.\boldsymbol{G}'}^{-1}(\boldsymbol{q}, E_i - E_f)] n_i (1 - n_f) + \frac{B_{fi}(\boldsymbol{q}+\boldsymbol{G})B_{fi}^*(\boldsymbol{q}+\boldsymbol{G}')}{|\boldsymbol{q}+\boldsymbol{G}|^2} \times \mathrm{Im}[-\epsilon_{\boldsymbol{G}.\boldsymbol{G}'}^{-1}(\boldsymbol{q}, E_f - E_i)] n_f (1 - n_i) \Bigg). \quad (4)$$

This is the result we were seeking for. The first term in parentheses accounts for out scatterings which lead to a decrease of the population n_i, where the Pauli-blocking term $(1-n_f)$ asserts that the final state of the scattering is unoccupied. This loss of population of n_i is accompanied by an increase of the population n_f, i.e., *in scatterings* described by

the second term. Thus, Eq. (4) describes a scattering-type process where population is transferred from the initial state i to the final state f. Comparison of Eqs. (1) and (4) reveals that the GW self-energy can indeed be interpreted in terms of a scattering process. Finally, we introduce the differential cross section

$$P_i(\omega) = \frac{1}{\pi^2}\sum_f \int_{\mathrm{BZ}} d\boldsymbol{q} \sum_{\boldsymbol{G}\boldsymbol{G}'} \frac{B_{if}(\boldsymbol{q}+\boldsymbol{G})B_{if}^*(\boldsymbol{q}+\boldsymbol{G}')}{|\boldsymbol{q}+\boldsymbol{G}|^2} \times \mathrm{Im}[-\epsilon^{-1}_{\boldsymbol{G}\boldsymbol{G}'}(\boldsymbol{q},\omega)]\delta(\omega - E_i + E_f), \quad (5)$$

which gives the probability that in the hot-electron scattering the energy ω is exchanged. Apparently, the total scattering rate must be given by the sum over all transition probabilities, i.e., $\tau_i^{-1} = \int_0^{E_i - E_F} d\omega P_i(\omega)$, as can be easily verified by insertion of Eq. (5).

A. Local fields

Let us analyze the various contributions to Eq. (1) in slightly more detail. The overlap matrix elements B_{if} account for the fact that the electron wavefunctions are not just plane waves, but have an additional Bloch part $u_{n\boldsymbol{k}}(\boldsymbol{r})$ with lattice periodicity. It can be readily shown that[7,41]

$$B_{if}(\boldsymbol{q}+\boldsymbol{G}) = \frac{1}{\Omega}\int_{\Omega} d\boldsymbol{r}\phi^*_{n_i\boldsymbol{k}}(\boldsymbol{r})e^{-i(\boldsymbol{q}+\boldsymbol{G})\boldsymbol{r}}\phi_{n_f\boldsymbol{k}+\boldsymbol{q}}(\boldsymbol{r}), \quad (6)$$

where the integral extends over the unit cell Ω. The initial electron state is characterized by the band index n_i and the wave vector $\boldsymbol{k}$, and the final one by the band index n_f and the wave vector $\boldsymbol{k}+\boldsymbol{q}$. This overlap matrix element describes how the hot electron couples to the charge fluctuations of the metal electrons. The propagation of the charge fluctuation is described by the inverse dielectric function, which, as shown in the Appendix, can be expressed through the density-density correlation function. Because the problem under consideration is homogeneous, in the propagation of a density fluctuation with wave vector $\boldsymbol{q}$ no fluctuations with different wave vectors can be induced. However, no corresponding conclusions apply for fluctuations with reciprocal lattice wave vectors $\boldsymbol{G}$ and $\boldsymbol{G}'$ which become coupled. This is a genuine solid-state effect absent in a homogeneous electron gas, and is known as the crystalline local-field effect (other local-field effects attributed to the Pauli and Coulomb hole[5,42] exist, which will not be considered in this work). To estimate the importance of local-field effects, we shall find it convenient to compare the results obtained from Eq. (1) with those where local-field effects are neglected by setting $\boldsymbol{G}=\boldsymbol{G}'$. Within this approximation, we can invert the dielectric function and obtain

$$\tau_i^{-1} \cong \frac{1}{\pi^2}\sum_f \int_{\mathrm{BZ}} d\boldsymbol{q}\sum_{\boldsymbol{G}} \frac{|B_{if}(\boldsymbol{q}+\boldsymbol{G})|^2\,\mathrm{Im}[\epsilon_{\boldsymbol{G}\boldsymbol{G}}(\boldsymbol{q},\omega)]}{|(\boldsymbol{q}+\boldsymbol{G})\epsilon_{\boldsymbol{G}\boldsymbol{G}}(\boldsymbol{q},\omega)|^2}, \quad (7)$$

with $\omega = E_i - E_f$ the inelasticity of the scattering. Occasionally we shall replace the dielectric function in the denominator by the static dielectric function $\epsilon_{\boldsymbol{G}\boldsymbol{G}}(\boldsymbol{q},0)$, and shall refer to this approximation as a static one.

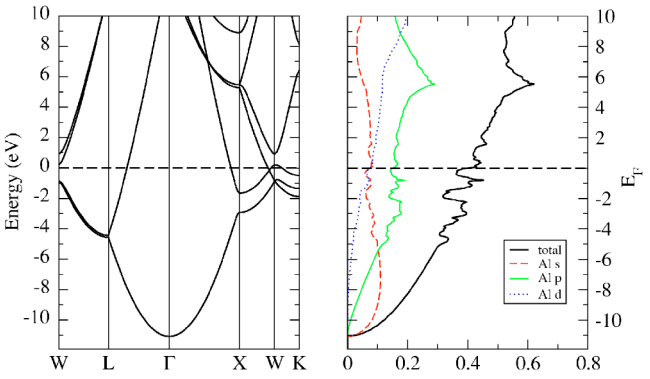

FIG. 1. (Color online) Band-structure (left panel) and density-of-states (right panel) plots for aluminium as calculated within the LAPW method.

B. Electron gas

For an electron injected into a homogeneous electron gas with an excess energy E_i close to the Fermi energy E_F, the hot-electron lifetimes can be approximately computed according to[2,6]

$$\tau^{-1} \cong 0.038 r_s^{5/2}(E_i - E_F)^2 \mathrm{eV}^{-2}\ \mathrm{fs}^{-1}, \quad (8)$$

where r_s is the usual electron-gas parameter[2,4] defined for an electron density n through $n = 4\pi r_s^3/3$, and the excess energy is supposed to be given in eV. The functional dependence of τ^{-1} on the excess energy can be easily understood from an analysis of the differential cross section $P_i(\omega)$. For the homogeneous electron gas, $P_i(\omega)$ can be obtained in a similar fashion to Eq. (5) from the integrand of Eq. (7) for constant overlap matrix elements. We next put forward a simple rea-

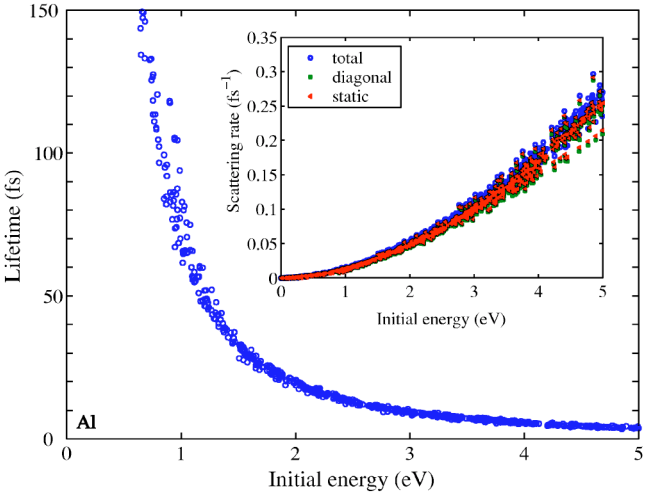

FIG. 2. (Color online) Hot electron lifetimes in aluminium as computed from Eq. (1) by including local field effects and dynamic screening. The inset shows the total scattering rate τ^{-1}. The symbols + and ◁ report the scattering rates which are obtained by neglecting local field effects and using a static approximation for the screening, respectively. The results clearly reveal a minor importance of local-field effects and dynamic screening, and support the electron-gas description of hot-electron scatterings in aluminium.

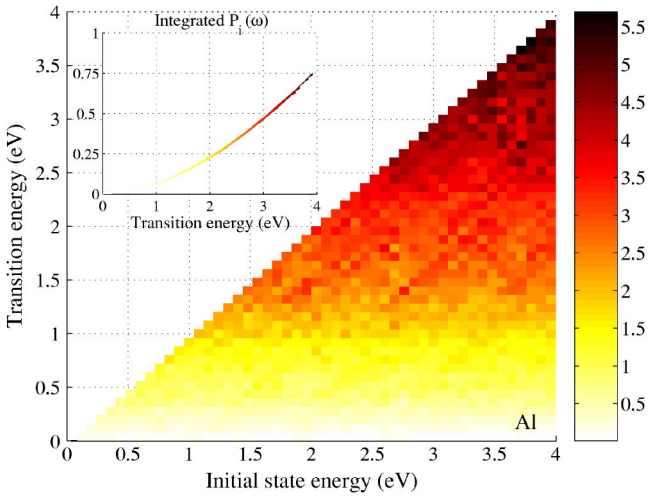

FIG. 3. (Color online) Intensity plot of the averaged differential cross section $P_i(\omega)$ in arbitrary units for the hot electron transitions in aluminium. The intensity of each square corresponds to the magnitude of the corresponding cross section. The inset reports the integrated differential cross section as a function of the energy ω transferred in the transitions.

soning which allows one to grasp the essentials of Eq. (8) on qualitative grounds: owing to the small momentum dependence of the screened Coulomb matrix elements, for a given $\omega \ll E_F$ the scattering rates are completely governed by the phase space $\mathrm{Im}\,\epsilon(\omega) \propto 4\pi E_F^2 \omega$ of electrons inside the Fermi sea which can act as scattering partners for the hot electron. Thus,

$$\tau_i^{-1} \propto \int_0^{E_i - E_F} d\omega \omega \propto (E_i - E_F)^2 \tag{9}$$

is the approximate energy dependence of the hot-electron scattering rates—in accordance to Eq. (8) which is derived within a more detailed approach. In the following we shall explore the influence of band structure effects on the simple $P_i(\omega) \propto \omega$ dependence expected from the electron-gas model.

III. RESULTS

In our calculations we start from band structure calculations based on density functional theory in the local-density approximation,[32] which are performed with a linearized-

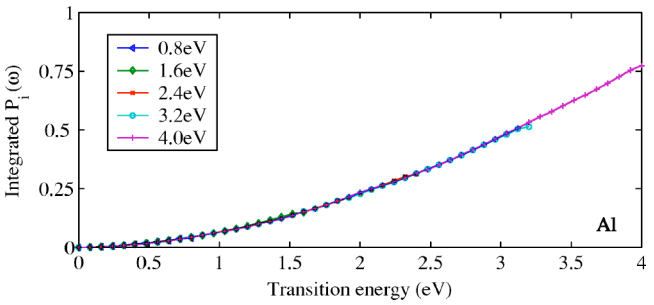

FIG. 4. (Color online) Integrated differential cross section in arbitrary units for different initial state energies and for aluminium.

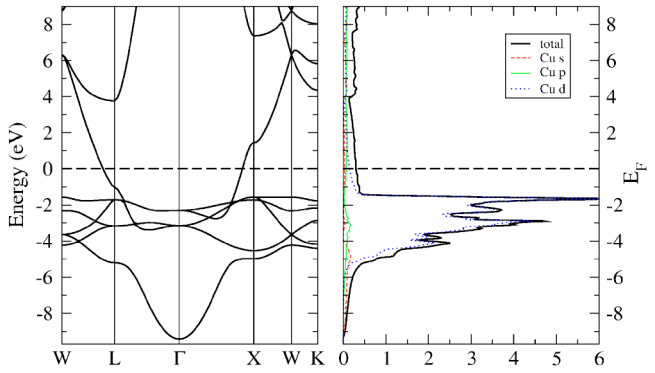

FIG. 5. (Color online) Band-structure (left panel) and density-of-states (right panel) plot for copper as calculated within the LAPW method.

augmented-plane-wave basis (LAPW) by use of the WIEN code.[31] For this LAPW basis the computation of the overlap matrix elements B_{if} turned out to be the most time-consuming part. To account for the localized *d*-band states in noble metals, within the atomic spheres an expansion of plane waves into spherical harmonics and spherical Bessel functions has to be performed by use of the Rayleigh expansion.[41] In our calculations we use an equidistant *k* mesh with typically $20 \times 20 \times 20$ points and expand the dielectric matrix in a plane-wave basis set.[41] All pertinent parameters of our computational approach were chosen on the basis of careful convergence tests.[43]

A. Aluminium

Because of the free-electron-like dispersion (see Fig. 1) aluminium is expected to exhibit hot-electron lifetimes and scattering rates reminiscent of the homogeneous electron gas, with only moderate deviations due to band structure effects.[8,44–47] Figure 2 shows hot-electron lifetimes as computed from Eq. (1) for different initial states. One clearly observes the energy dependence $\tau \propto (E_i - E_F)^{-2}$ of hot-electron lifetimes, as expected on the basic grounds of Eq. (9) for the homogeneous electron gas. For an electron gas parameter $r_s = 2.07$ representative for aluminium and an ex-

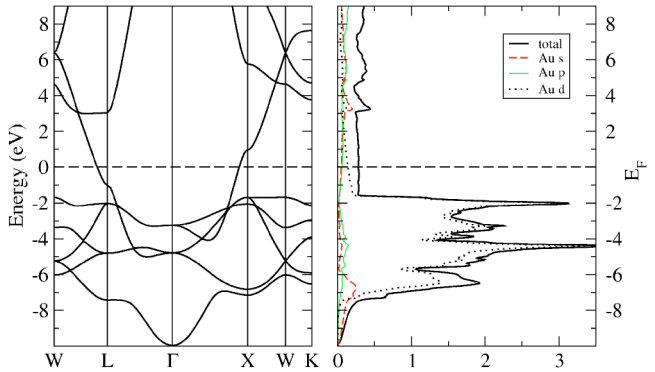

FIG. 6. (Color online) Band-structure (left panel) and density-of-states (right panel) plot for gold as calculated within the LAPW method.

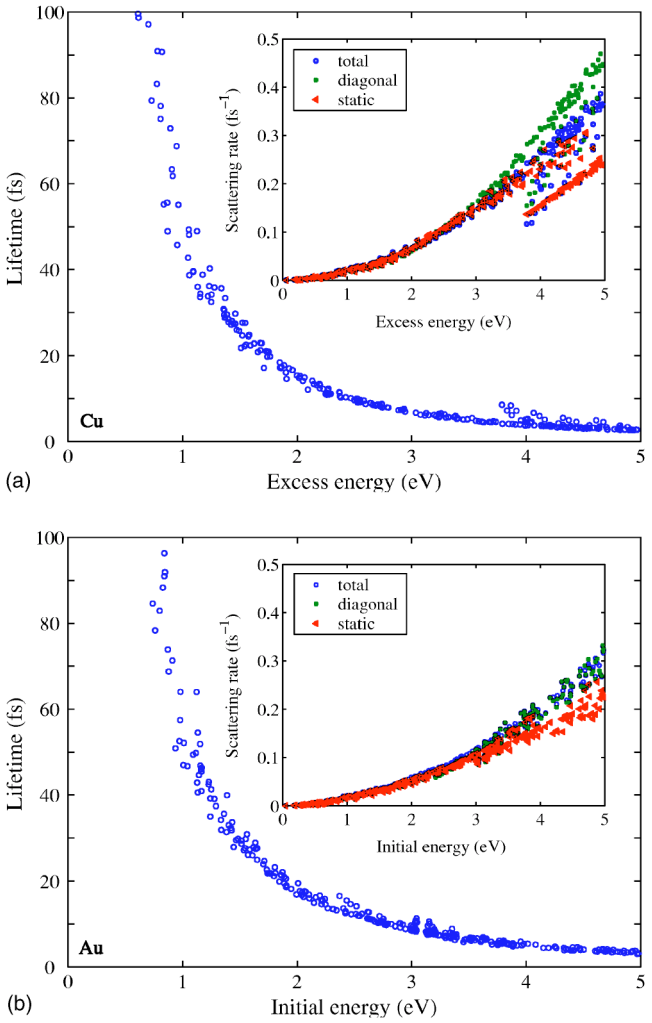

FIG. 7. (Color online) Hot-electron lifetimes for copper (top) and gold (bottom) as computed from Eq. (1). For details see figure caption 2.

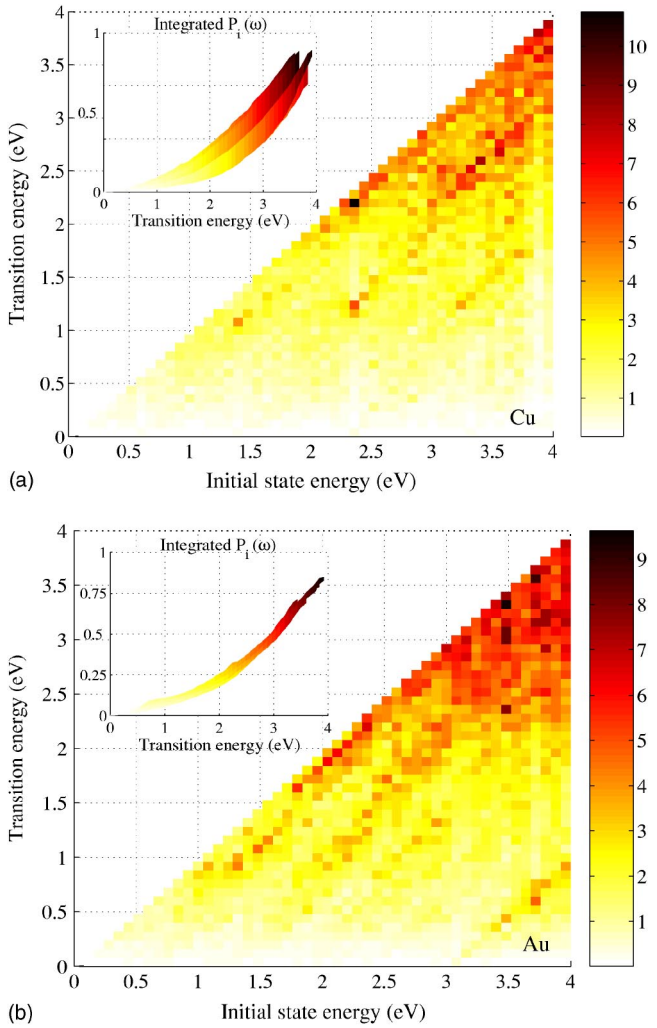

FIG. 8. (Color online) Same as Fig. 3 but for copper (top) and gold (bottom).

cess energy of 1 eV we obtain from Eq. (8) a hot-electron lifetime of 42.7 fs—to be compared with the value of approximately 60–70 fs of our LAPW band structure calculations. This discrepancy has been discussed in the literature with some controversy.[7,16]

In the following we use the interpretation of Eq. (1) as a scattering process where the hot electron is scattered from an initial to a final state. The differential cross section $P_i(\omega)$ introduced in Eq. (5) gives the probability that in a hot-electron scattering the energy ω is exchanged. Figure 3 shows a density plot of $P_i(\omega)$ as obtained by averaging over all initial states i of the Brillouin zone with energy E_i and over all final states f with energy $E_f=E_i-\omega$. Because E_i-E_F is the largest energy that can be exchanged in a scattering process, the differential cross section $P_i(\omega)$ is nonzero only for $\omega<E_i-E_F$. We observe that the differential cross section has an energy dependence according to $P_i(\omega)\propto\omega$, as expected from the electron-gas result (9). This is seen even more clearly in the inset of Fig. 3 which reports the integrated transition probability $\int_0^\omega d\omega' P_i(\omega')$ for all initial states i. For the electron gas, where the differential cross section $P_i(\omega)$ of Eq. (9) does not depend on the initial state i (with exception of the above-mentioned energy cutoff $\omega<E_i-E_F$), this quantity exhibits a simple ω^2 dependence. Indeed, such behavior is clearly seen in Fig. 3 as well as in Fig. 4, which reports the integrated differential cross section for five selected hot-electron energies E_i, where again all curves lie almost perfectly on top of each other. In conclusion, our results demonstrate that the electron-gas model provides an excellent qualitative explanation of the hot-electron scattering characteristics in aluminium, and band structure effects are only responsible for moderate quantitative deviations.

B. Gold and copper

Things become considerably more complicated for the noble metals copper and gold. The band structure of these two materials depicted in Figs. 5 and 6 has a striking similarity: a few electron volt below the Fermi energy there is a huge density-of-states associated to d bands, and the states above the Fermi energy have strong sp and minor d characteristics. Figure 7 shows the hot-electron lifetimes as computed from Eq. (1) for copper and gold. Let us first concen-

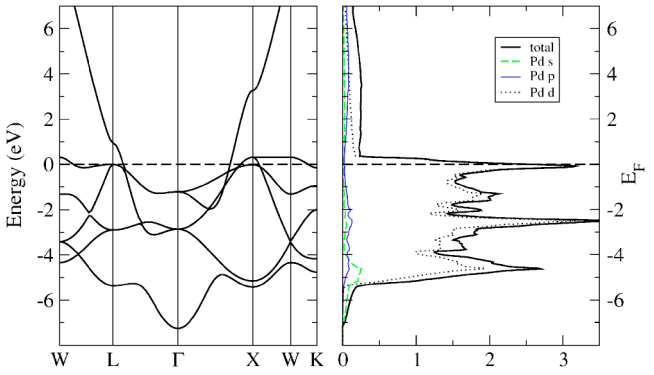

FIG. 9. (Color online) Band-structure (left panel) and density-of-states (right panel) plot for palladium as calculated within the LAPW method.

trate on the excess energies $E_i - E_F$ below approximately 4 eV. The hot-electron lifetimes show the expected $(E_i - E_F)^2$ behavior. However, as compared to the electron-gas results for gold (e.g., $\tau \sim 17$ fs for an excess energy of 1 eV) the hot-electron lifetimes in Fig. 7 are enhanced by a factor of almost 4, where similar conclusions apply for copper.[6,7] This strong enhancement of hot-electron lifetimes is attributed in accordance to Campillo *et al.*[6,7] to *d*-band screening, where the high *d*-band density of states below the Fermi energy results in efficient screening contributions. However, in contrast to the pseudopotential results presented by Campillo *et al.*,[8] our all-electron results obtained within an LAPW basis exhibit only a small influence of local-field effects and static screening on the hot-electron lifetimes, as shown in the insets of Fig. 7.

From the inspection of the band structure and density-of-states plots of Figs. 5 and 6 one might expect that above an excess energy of approximately 2 eV an additional scattering channel opens for the hot electron, where the partner electrons are promoted from *d* bands below the Fermi energy to

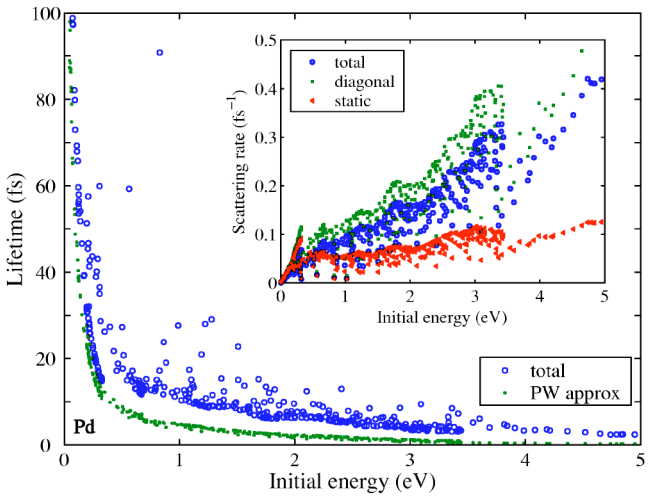

FIG. 10. (Color online) Hot electron lifetimes in palladium as computed from Eq. (1). The inset shows the total scattering rate τ^{-1} and the symbols + and ◁ report the scattering rates which are obtained by neglecting local field effects and using a static approximation for the screening, respectively. For details see text.

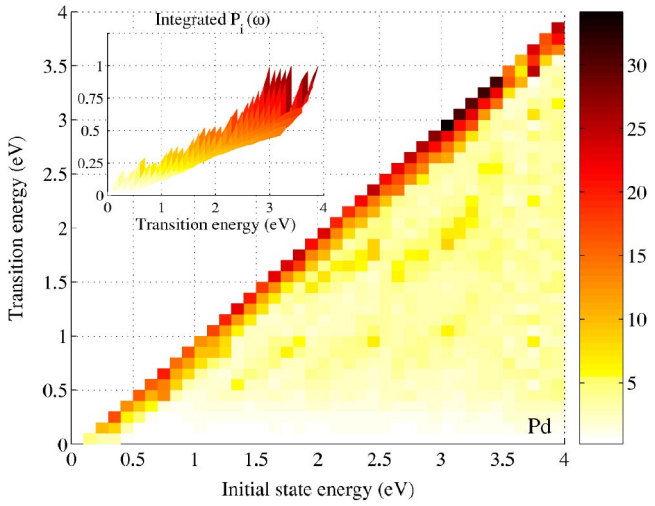

FIG. 11. (Color online) Same as Fig. 3 but for palladium.

states above E_F. This would result in an abrupt and strong decrease of τ_i. Such behavior is clearly neither seen in Fig. 7, nor in the differential cross sections shown in Fig. 8 where no substantial enhancement of $P_i(\omega)$ at the onset of possible *d*-band scatterings is present. The reason is that for scatterings where the initial and final state of the scattering partner have different symmetries, i.e., *d* like versus *sp* like, the resulting overlap matrix elements are vanishingly small, and correspondingly the contributions to the hot-electron lifetimes become strongly suppressed. As compared to the results of aluminium, the integrated differential cross sections reported in the insets of Fig. 8 exhibit a stronger dependence on the initial state energies, as apparent from the broadening of the curves. This is due to the more complex band structure and the complicated interplay of the overlap matrix elements and the dynamic form factor in Eq. (5). Finally, in copper and gold a second band for initial hot-electron states opens above approximately 4 eV, i.e., at the *L* point shown in Figs. 5 and 6, within which the scattering characteristics is substantially different. To summarize, the hot-electron lifetimes in copper and gold exhibit the expected $(E_i - E_F)^{-2}$ dependence, and only the absolute values of hot-electron lifetimes are strongly altered with respect to the electron-gas result (8) because of *d*-band screening.

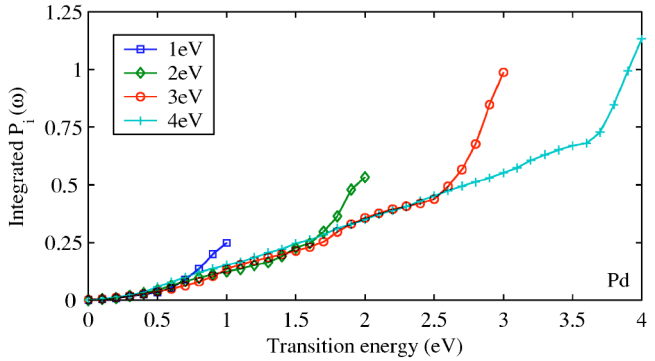

FIG. 12. (Color online) Integrated differential cross section in arbitrary units for different initial state energies and for palladium.

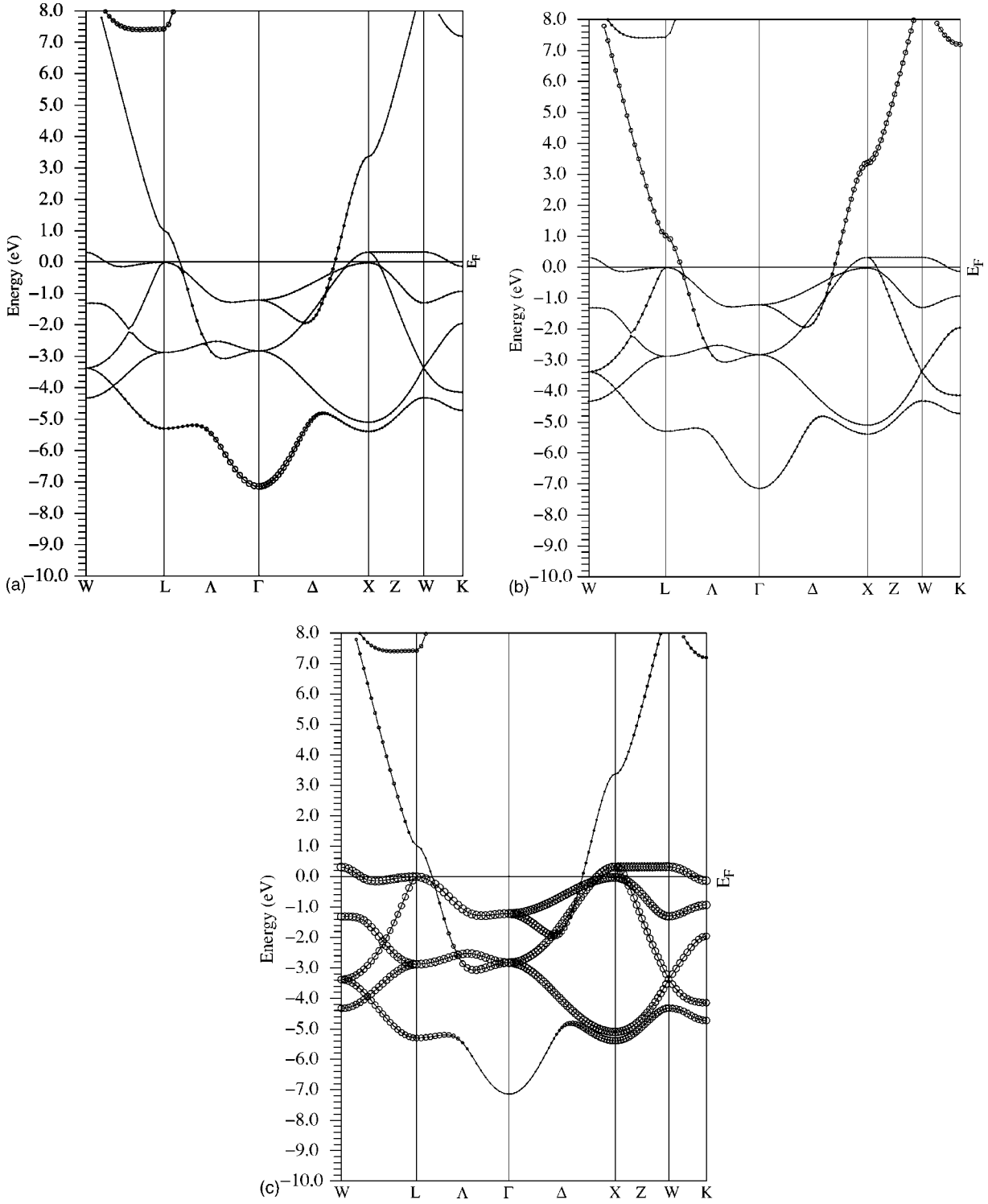

FIG. 13. (a) *s*-like, (b) *p*-like, and (c) *d*-like band characteristics for palladium. The sizes of the circles indicate the degree of *s*, *p*, and *d*-like characteristics for a given $\boldsymbol{k}$ point.

C. Palladium

The band structure of palladium depicted in Fig. 9 is similar to those of copper and gold, with the important difference that the *d* bands cross the Fermi energy. As we shall discuss in the following, this opens the possibility for efficient *d*-band scatterings and results in a strong alteration of the lifetime characteristics, which no longer can be explained within the electron-gas model. Figure 10 reports the hot-electron lifetimes as computed from Eq. (1) for different initial energies. One clearly observes that τ_i does not follow at all the $(E_i - E_F)^{-2}$ dependence predicted by the electron-gas model (with the exception of states very close to the Fermi

level where the quadratic energy dependence of the self energy remains valid).

Details of the scattering process are depicted in Fig. 11 which reports the differential cross section $P_i(\omega)$ for different initial energies E_i. $P_i(\omega)$ is strongly enhanced for the largest transition energies $\omega=E_i-E_f$ where the hot electron is scattered to a final *d*-band state above E_F. Indeed, the width of the region where $P_i(\omega)$ is substantially enhanced directly corresponds to the narrow energy window of *d*-band states above E_F depicted in Fig. 9. To understand the details of the underlying scattering process, in Fig. 13 we plot the *s*, *p*, and *d* character of the band structure. While hot-electron states slightly above E_F have a dominant *sp* character, those at lower energies have a dominant *d* character. Quite generally, such different characteristics of initial and final states results in very small transition probabilities because of the small overlap matrix elements B_{if}, as previously seen at the examples of copper and gold. However, since all hot-electron states have a small *d* admixture there exists a small, but nonvanishing transition probability to the final *d*-like states. Because of the extremely high *d*-band density-of-states around E_F, this gives rise to an additional scattering channel with a significant impact on the hot-electron lifetimes. A quantitative estimate can be obtained from Fig. 12 which reports the integrated differential cross section for four selected initial states. Within the narrow energy window of *d*-band states above E_F, the integrated $P_i(\omega)$ is approximately doubled. Thus, scatterings within the *sp* bands and scatterings from an initial *sp*- to a final *d*-band state are of equal importance.

There exist other interesting effects associated to *d*-band transitions. First, in Fig. 10 one observes that for certain initial states the hot-electron lifetimes are strongly enhanced. A closer analysis reveals that these states are associated to high-symmetry *k* points of the Brillouin zone, e.g., the *L* or *X* point, where, as shown in Fig. 13, the *d*-character becomes almost zero. Correspondingly, the scattering to the final *d*-band states is strongly suppressed and the hot-electron lifetime strongly enhanced. Further support for this interpretation is provided by the "plane-wave" (PW)[6] results shown in Fig. 10, which are obtained by setting all overlap matrix elements B_{if} in Eq. (1) equal to 1. The corresponding hot-electron lifetimes clearly exhibit a much smoother energy dependence, thus demonstrating the important role of the overlap matrix elements. A second effect associated to the *d* bands can be observed in the inset of Fig. 10 where the hot-electron scattering rate as a function of energy increases stepwise. A comparison of this figure with the carrier density-of-states depicted in Fig. 9 shows that the steps occur at those energies where the *d*-band density-of-states has peaks. This can be understood as follows. Since the energy exchanged in a scattering of the hot electron to a *d*-band state is approximately $\omega\sim E_i-E_F$, the scattering partner has to be scattered from a state with energy E' below the Fermi energy to a state with energy $E'+\omega$ above E_F. Because of the high *d*-band density-of-states above E_F, the partner electron will preferentially end up in a *d*-band state with an energy close to E_F. Thus, $E'+\omega\sim E_F$, and accordingly $E'\sim 2E_F-E_i$ is the initial energy of the partner electron. Since the differential cross section of the corresponding transition is proportional to the carrier density-of-states $g(E')$ of partner electrons, the total cross section is a quite direct measure of $\sim g(2E_F-E_i)$, and thus explains the strong correlation between τ_i^{-1} and the carrier density-of-states below E_F. We finally emphasize the large influence of local-field effects and dynamic screening on the hot-electron lifetimes, as depicted in the inset of Fig. 10. This clearly shows that an accurate band structure description is indispensable for the calculation of hot-electron lifetimes.

IV. CONCLUSIONS

In conclusion, we have analyzed hot-electron scatterings in metals within a first-principles approach based on density-functional-theory band structure calculations and on Green function calculations within the *GW* approximation. It has been shown that the self-energy can be interpreted in terms of a scattering process, where the hot electron is scattered from an initial to a final state. For aluminium the homogeneous electron-gas model provides a good description of both the lifetimes and the differential cross section. In copper and gold, the large *d*-band density of states below the Fermi energy E_F is responsible for a strong enhancement of hot-electron lifetimes. Finally, for palladium the *d* bands around E_F lead to a drastic modification of the lifetimes and the scattering characteristics in comparison to the predictions of the homogeneous electron-gas model. Our results provide further support for the *GW* approximation scheme that has recently proven particularly successful in the first-principles description of excited-state properties in metals and semiconductors. In this work we have employed the most simple description scheme based on the G_0W_0 and mass-shell approximations. More sophisticated schemes are expected to introduce moderate modifications without substantially changing the qualitative behavior. Future work should also address description schemes beyond *GW* to account for the enhanced correlation effects of localized *d*-band electrons in palladium.

ACKNOWLEDGMENTS

We are grateful to Pedro de Andres, Fernando Flores, and Kathrin Glantschnig for most helpful discussions, and thank Sangeeta Sharma for a careful reading of the manuscript. This work has been supported in part by the EU under the TMR network "EXCITING" and the Austrian science fund FWF under Project No. P16227.

APPENDIX

In this appendix we present the details of deriving Eq. (4) within the density-matrix framework. Consider an operator *A* acting upon the hot-electron degrees of freedom solely, whose expectation value is given by $\langle A(t)\rangle=\mathrm{tr}[\rho(t)A(t)]$. When we expand the double commutator in Eq. (2) and make use of the cyclic permutation under the trace we get

$$\langle \dot{A}(t)\rangle \cong -\int_{t_0}^{t} dt'[\langle A(t)H'(t)H'(t')\rangle + \langle H'(t')H'(t)A(t)\rangle - \langle H'(t)A(t)H'(t')\rangle - \langle H'(t')A(t)H'(t)\rangle]. \quad \text{(A1)}$$

This expression has a very precise meaning in the context of the master equation in Lindblad form,[37,48] where the first two terms in parentheses account for out scatterings and the remaining ones for in scatterings. As we shall see, analogous conclusions apply for hot electrons in metals. To compute the loss of population of the initial state we evaluate Eq. (A1) for the number operator $c_i^\dagger c_i$ and use according to Eq. (3)

$$H' \cong \sum_f \int d\boldsymbol{r} d\boldsymbol{r}' \frac{[B_{if}(\boldsymbol{r})c_i^\dagger c_f + B_{if}^*(\boldsymbol{r})c_f^\dagger c_i]\hat{n}(\boldsymbol{r}')}{|\boldsymbol{r}-\boldsymbol{r}'|}, \quad \text{(A2)}$$

for the Coulomb coupling of the hot electron with the metal electrons; here $B_{if}(\boldsymbol{r})=\phi_i^*(\boldsymbol{r})\phi_f(\boldsymbol{r})$ is the overlap matrix element. The random-phase approximation, which assumes that the density fluctuation of the hot electron moves independently of $\hat{n}(\boldsymbol{r}')$, then translates to $[c_i,\hat{n}(\boldsymbol{r}')]=0$ and $[c_f,\hat{n}(\boldsymbol{r}')]=0$. Inserting expression (A2) into Eq. (A1) gives after some straightforward calculation

$$\dot{n}_i \cong -2\,\mathrm{Re}\int_{t_0}^{t} dt' \int d\boldsymbol{\tau} B_{if}(\boldsymbol{r})B_{if}^*(\overline{\boldsymbol{r}})e^{i(E_i-E_f)(t-t')} \times \frac{\langle c_i^\dagger c_f c_f^\dagger c_i \hat{n}(\boldsymbol{r}',t)\hat{n}(\overline{\boldsymbol{r}}',t')\rangle_0}{|\boldsymbol{r}-\boldsymbol{r}'||\overline{\boldsymbol{r}}-\overline{\boldsymbol{r}}'|} + (i\leftrightarrow f), \quad \text{(A3)}$$

where $d\boldsymbol{\tau}$ denotes the integration over $\boldsymbol{r}$, $\boldsymbol{r}'$, $\overline{\boldsymbol{r}}$, and $\overline{\boldsymbol{r}}'$, $\langle\cdots\rangle_0$ is the expectation value for the initial density operator ρ_0, and the second term follows from the first one by exchanging i and f. In deriving this expression we have assumed that the time evolution of c_i and c_f is solely according to H_0, which is similar to the G_0W_0 approximation of the Green function approach. The expectation value can be factorized into $n_i(1-n_f)\langle\hat{n}(\boldsymbol{r}',t)\hat{n}(\overline{\boldsymbol{r}}',t')\rangle_0$, where the last term is known as the dynamic form factor[3,42] $S(\boldsymbol{r}',\overline{\boldsymbol{r}}',t-t')$. This is the point where we meet with the corresponding Green function calculation. It is worth emphasizing the simplicity of our present derivation, which solely required the general master equation (2) in Born approximation together with the Coulomb coupling (A2) in random-phase approximation—to be contrasted with the whole machinery of auxiliary functions invoked in the corresponding Green function approach. Equation (A3) has the obvious structure that at time t' the hot electron becomes correlated with a density fluctuation $\hat{n}(\overline{\boldsymbol{r}}',t')$ of the metal, where the coupling strength is given by the overlap matrix element $B_{if}^*(\overline{\boldsymbol{r}})$; the scattered electron and the density fluctuation move independently of each other, as described by the exponential and the dynamic form factor; and finally, at time t the propagated density fluctuation $\hat{n}(\boldsymbol{r}',t)$ acts back on the hot electron, where again the coupling strength is given by $B_{if}(\boldsymbol{r})$. Because of the finite interaction time the hot electron can transfer energy to the metal electrons, and becomes scattered from the initial state i to the final state f. The response of the metal electrons is fully described by the dynamic form factor $S(\boldsymbol{r},\boldsymbol{r}';t-t')$, which is a measure of how much of a density fluctuation created at time t' and position $\boldsymbol{r}'$ is left in the system at a later time t and a different position $\boldsymbol{r}$. This function is closely related to the density-density correlation function[42]

$$L(\boldsymbol{r},\boldsymbol{r}';t) = -i\theta(t)\langle[\hat{n}(\boldsymbol{r},t),\hat{n}(\boldsymbol{r}',0)]\rangle_0, \quad \text{(A4)}$$

which accounts for the propagation of density fluctuations. By inserting a complete set of eigenstates of H_0+H'' in between the density fluctuation operators $\hat{n}$, we can establish a relation between L and S:[4,5,42]

$$L(\boldsymbol{r},\boldsymbol{r}';\omega) = \int_{-\infty}^{\infty} \frac{d\omega'}{2\pi} \frac{S(\boldsymbol{r},\boldsymbol{r}';\omega') - S(\boldsymbol{r}',\boldsymbol{r};-\omega')}{\omega-\omega'+i0}. \quad \text{(A5)}$$

At zero temperature $S(\boldsymbol{r}',\boldsymbol{r};-\omega)$ vanishes because the metal can only absorb energy. Thus, $\mathrm{Im}\,L(\boldsymbol{r},\boldsymbol{r}',\omega) = -\mathrm{Re}\,S(\boldsymbol{r},\boldsymbol{r}';\omega)/2$. We next follow Refs. 6–8 and 33 and consider in Eq. (A3) only the real part of $S(\boldsymbol{r},\boldsymbol{r}';\omega)$. Within this approximation the hot-electron lifetime τ^{-1} of Eq. (1) is computed on the "mass shell," i.e., for the unrenormalized single-particle energies E_i and E_f, which is known to be a well-controlled approximation.[17] Our remaining task is to compute the density-density correlation function within the random-phase approximation. To this end, we introduce the irreducible polarization[4,5] $P(\boldsymbol{r},\boldsymbol{r}';t-t')$ which is related to the density-density correlation function through $L=P+PVL$, where V is the bare Coulomb potential and the different quantities are supposed to be connected through a convolution in time and space. Within the random-phase approximation the polarization function becomes[4,5,39,42]

$$P(\boldsymbol{r},\boldsymbol{r}';t) = -i\theta(t)\langle[e^{iH_0t}\hat{n}(\boldsymbol{r})e^{-iH_0t},\hat{n}(\boldsymbol{r}')]\rangle_0. \quad \text{(A6)}$$

We finally define in accordance to Refs. 6–8 and 33 the dielectric function through $\epsilon=1-PV$ to bring Eq. (A3) to its final form of Eq. (4), together with[41]

$$\mathrm{Im}\,\epsilon_{\boldsymbol{G}\boldsymbol{G}'}(\boldsymbol{q},\omega) = \frac{1}{2\pi}\sum_{mn}\int_{BZ} d\boldsymbol{k} \frac{B_{nm}(\boldsymbol{q}+\boldsymbol{G})B_{nm}^*(\boldsymbol{q}+\boldsymbol{G}')}{|\boldsymbol{q}+\boldsymbol{G}'|^2} \times \delta(\omega+E_n-E_m), \quad \text{(A7)}$$

where m denotes an occupied state with wavevector $\boldsymbol{k}$ and n and unoccupied one with wave vector $\boldsymbol{k}+\boldsymbol{q}$. The real part of the dielectric function is obtained by use of the Kramers-Kronig relation.

*Electronic address: ulrich.hohenester@uni-graz.at
†Present address: Institut für Wärmetechnik, TU Graz, Inffeldgasse 25/B, 8010 Graz, Austria.

[1] J. J. Quinn, Phys. Rev. **112**, 812 (1958).
[2] J. J. Quinn, Phys. Rev. **126**, 1453 (1962).
[3] P. Nozières, *Theory of Interacting Fermi Systems* (Benjamin, New York, 1964).
[4] A. L. Fetter and J. D. Walecka, *Quantum Theory of Many-Particle Systems* (McGraw-Hill, New York, 1971).
[5] G. D. Mahan, *Many-Particle Physics* (Plenum, New York, 1981).
[6] I. Campillo, V. M. Silkin, J. M. Pitarke, A. Rubio, E. Zarate, and P. M. Echenique, Phys. Rev. Lett. **83**, 2230 (1999).
[7] I. Campillo, V. Silkin, J. M. Pitarke, E. Chulkov, A. Rubio, and P. M. Echenique, Phys. Rev. B **61**, 13 484 (2000).
[8] I. Campillo, J. M. Pitarke, A. Rubio, and P. M. Echenique, Phys. Rev. B **62**, 1500 (2000).
[9] V. P. Zhukov, F. Aryasetiawan, E. V. Chulkov, and P. M. Echenique, Phys. Rev. B **65**, 115116 (2002).
[10] V. P. Zhukov, E. V. Chulkov, and P. M. Echenique, Phys. Rev. B **68**, 045102 (2003).
[11] V. P. Zhukov, F. Aryasetiawan, E. V. Chulkov, I. G. de Gurtubay, and P. M. Echenique, Phys. Rev. B **64**, 195122 (2001).
[12] A. García-Lekue, J. M. Pitarke, E. V. Chulkov, A. Liebsch, and P. M. Echenique, Phys. Rev. B **68**, 045103 (2003).
[13] L. Hedin and S. Lundqvist, Solid State Phys. **23**, 1 (1969).
[14] F. Aryasetiawan and O. Gunnarson, Rep. Prog. Phys. **61**, 237 (1998).
[15] G. Onida, L. Reining, and A. Rubio, Rev. Mod. Phys. **74**, 601 (2002).
[16] W.-D. Schöne, R. Keyling, M. Bandic, and W. Eckardt, Phys. Rev. B **59**, 5926 (1999).
[17] R. Keyling, W.-D. Schöne, and W. Ekardt, Phys. Rev. B **61**, 1670 (2000).
[18] M. R. Bacelar, W.-D. Schöne, R. Keyling, and W. Ekardt, Phys. Rev. B **66**, 153101 (2002).
[19] A. Marini, R. Del Sole, A. Rubio, and G. Onida, Phys. Rev. B **66**, 161104 (2002).
[20] F. Ladstädter, P. de Pablos, U. Hohenester, P. Puschnig, C. Ambrosch-Draxl, P. L. de Andres, F. Garcia-Vidal, and F. Flores, Phys. Rev. B **68**, 085107 (2003).
[21] S. Sze, C. Crowell, and E. Labate, J. Appl. Phys. **37**, 2690 (1966).
[22] A. Goldmann, W. Altmann, and V. Dose, Solid State Commun. **79**, 511 (1991).
[23] H. Petek and S. Ogawa, Prog. Surf. Sci. **56**, 239 (1997).
[24] L. D. Bell and W. J. Kaiser, Phys. Rev. Lett. **61**, 2368 (1988).
[25] P. L. de Andres, F. J. Garcia-Vidal, K. Reuter, and F. Flores, Prog. Surf. Sci. **66**, 3 (2001).
[26] K. Reuter, P. L. de Andres, F. J. Garcia-Vidal, F. Flores, U. Hohenester, and P. Kocevar, Europhys. Lett. **45**, 181 (1999).
[27] K. Reuter, U. Hohenester, P. L. de Andres, F. Garcia-Vidal, F. Flores, K. Heinz, and P. Kocevar, Phys. Rev. B **61**, 4522 (2000).
[28] P. F. de Pablos, F. J. Garcia-Vidal, F. Flores, and P. L. de Andres, Phys. Rev. B **66**, 075411 (2002).
[29] L. D. Bell, Phys. Rev. Lett. **77**, 3893 (1996).
[30] R. Ludeke and A. Bauer, Phys. Rev. Lett. **71**, 1760 (1993).
[31] P. Blaha, K. Schwarz, and J. Luitz, *WIEN97, A Full Potential Linearized Augmented Plane Wave Package for Calculating Crystal Properties* (Universität Wien, Vienna, 1999).
[32] R. M. Dreizler and E. U. Gross, *Density Functional Theory* (Springer, Berlin, 1990).
[33] P. M. Echenique, J. M. Pitarke, E. V. Chulkov, and A. Rubio, Chem. Phys. **251**, 1 (2000).
[34] F. Rossi and T. Kuhn, Rev. Mod. Phys. **74**, 895 (2002).
[35] E. Fick and G. Sauermann, *The Quantum Statistics of Dynamic Processes* (Springer, Berlin, 1990).
[36] L. E. Reichl, *Statistical Physics* (Wiley, New York, 1998).
[37] D. F. Walls and G. J. Millburn, *Quantum Optics* (Springer, Berlin, 1995).
[38] R. Balescu, *Statistical Mechanics of Charged Particles* (Interscience, New York, 1963).
[39] U. Hohenester and W. Pötz, Phys. Rev. B **56**, 13 177 (1997).
[40] U. Hohenester, Phys. Rev. B **64**, 205305 (2001).
[41] P. Puschnig and C. Ambrosch-Draxl, Phys. Rev. B **66**, 165105 (2002).
[42] K. S. Singwi and M. P. Tosi, Solid State Phys. **36**, 177 (1981).
[43] F. Ladstädter, Master thesis, Karl-Franzens-Universität, Graz, 2001.
[44] P. M. Platzman, E. D. Isaacs, H. Williams, P. Zschack, and G. E. Ice, Phys. Rev. B **46**, 12 943 (1992).
[45] W. Schulke, H. Schulte-Schrepping, and J. R. Schmitz, Phys. Rev. B **47**, 12 426 (1993).
[46] A. Fleszar, A. A. Quong, and A. G. Eguiluz, Phys. Rev. Lett. **74**, 590 (1995).
[47] B. C. Larson, J. Z. Tischler, E. D. Isaacs, P. Zschack, A. Fleszar, and A. G. Eguiluz, Phys. Rev. Lett. **77**, 1346 (1996).
[48] U. Hohenester, C. Sifel, and P. Koskinen, Phys. Rev. B **68**, 245304 (2003).